Journal of Solid State Chemistry **166,** 203–212 (2002)
doi:10.1006/jssc.2002.9583, available online at http://www.idealibrary.com on IDEAL®

Multianvil High-Pressure Syntheses and Crystal Structures of the New Rare-Earth Oxoborates χ-$DyBO_3$ and χ-$ErBO_3$

Hubert Huppertz,[1] Benjamin von der Eltz, Rolf-Dieter Hoffmann, and Holger Piotrowski

Department Chemie, Ludwig-Maximilians-Universität München, Butenandtstraße 5-13 (Haus D), 81377 München, Germany

Received December 12, 2001; in revised form February 28, 2002; accepted March 8, 2002

χ-$DyBO_3$ and χ-$ErBO_3$ were synthesized under high-pressure/high-temperature conditions from Dy_2O_3 (Er_2O_3) and boron oxide B_2O_3 in a Walker-type multianvil apparatus at 8 GPa and 1600 K. Both compounds crystallize with a pronounced subcell. Single crystal X-ray data of the normal cell yielded: $P\bar{1}$, $a = 724.0(1)$ pm, $b = 901.1(1)$ pm, $c = 987.2(1)$ pm, $\alpha = 81.40(2)°$, $\beta = 85.67(2)°$, $\gamma = 77.02(2)°$, $Z = 12$, $R1 = 0.0448$, $wR2 = 0.0922$ for χ-$DyBO_3$ and $a = 718.1(1)$ pm, $b = 897.1(1)$ pm, $c = 980.2(1)$ pm, $\alpha = 81.32(2)°$, $\beta = 85.54(2)°$, $\gamma = 77.11(2)°$, $Z = 12$, $R1 = 0.0452$, $wR2 = 0.0807$ for χ-$ErBO_3$. The compounds are isotypical and contain Ln^{3+}-ions (Ln = Dy, Er) as well as layers built up from the new non-cyclic $[B_3O_9]^{9-}$-anions, which exhibit one trigonal BO_3-(△) and two tetrahedral BO_4-groups (□) according to 1△2□:△2□. Temperature-resolved X-ray powder diffraction shows the metastable character of χ-$DyBO_3$. © 2002 Elsevier Science (USA)

Key Words: **high-pressure; multianvil; χ-$DyBO_3$; χ-$ErBO_3$; borates; crystal structure.**

1. INTRODUCTION

In the last years, oxoborate compounds have received a lot of attention due to their interesting physical properties, which make them attractive for numerous practical applications (1). The rare-earth orthoborates $LnBO_3$ exhibit polymorphism which led to a large number of studies concerning their crystallographic structures and chemical properties (2). These solids are characterized by a high structural flexibility caused in the linkage of planar/non-planar BO_3-groups and BO_4-tetrahedra, which can occur as isolated or condensed fundamental building units. As a general trend, Levin *et al.* (3) and Roth *et al.* (4) reported that the crystal structures of the rare-earth orthoborates are related to the three crystalline forms of $CaCO_3$, i.e., aragonite (λ-$LnBO_3$ with Ln = La–Sm), vaterite (π- and μ-$LnBO_3$ with Ln = Y, Ce–Nd, Sm–Lu) and calcite β-$LnBO_3$ (Ln = Sc, Yb, Lu). While the crystal structure solutions and refinements of the aragonite and calcite phases are not problematic, there have been numerous efforts devoted to the structure determinations of the vaterite phases and there are still considerable controversies left. First it was assumed, that the borate group in the vaterite phases revealed a triangular geometry. Later spectroscopic investigations showed, that these compounds contain only the cyclic $[B_3O_9]^{9-}$-group, which is built up by three BO_4-tetrahedra. Chadeyron *et al.* reinvestigated the crystal structure of YBO_3 using single-crystal data (5). They described a structure model which contains the $[B_3O_9]^{9-}$ unit with partial occupancy (1/3) of the boron position and one oxygen position which is very unlikely. Recently, Ren *et al.* (6) used electron diffraction on $GdBO_3$, by which several weak reflections were observed. At this stage, it was clear that the hexagonal cell of YBO_3 is only a subcell of the rhombohedral structure ($R32$), wherein the $[B_3O_9]^{9-}$-groups can be arranged in a way avoiding partial occupancies of oxygen and boron positions.

In the same work, Ren *et al.* described, that the high-temperature phase of $GdBO_3$ crystallizes in the hexagonal space group $P6_3/mmc$ leading to a calcite-related structure with isolated BO_3^{3-} units. Additionally, two different high-temperature forms denoted H-$LaBO_3$ and H-$NdBO_3$ have been found. According to Böhlhoff *et al.* (7), H-$LaBO_3$ crystallizes in the space group $P2_1/m$ with discrete planar BO_3-groups, whereas the triclinic H-$NdBO_3$ phase with non-equilateral BO_3-triangles was characterized by Palkina *et al.* (8).

Investigations concerning the behavior of the rare-earth orthoborates under high-pressure/high-temperature conditions were carried out by Meyer (9, 10) and Meyer and Skokan (11). Experiments covered a range up to a maximum pressure of 6.5 GPa and a temperature of 1300°C. They showed, that the rare-earth borates μ-$LnBO_3$ (Ln = Eu–Dy) transform into the H-$NdBO_3$ structure (ν-$LnBO_3$) under high-pressure/high-temperature conditions. In the case of ν-$SmBO_3$ and ν-$EuBO_3$, it was possible to reach the aragonite-structure by enhancement of pressure.

[1]To whom correspondence should be addressed. Fax.: (+49)-89-2180-7806. E-mail: huh@cup.uni-muenchen.de.

0022-4596/02 $35.00

Our research is aimed to extend the investigations so far done into regions of much higher pressure and temperature. In the following, we describe the syntheses and the structural properties of two new oxoborates. According to the designation of several polymorphs of the orthoborates with Greek letters by Meyer (9, 10) and Meyer and Skokan (11) the new polymorphs in this work were named χ-$Ln$$BO_3$ (Ln = Dy, Er).

2. EXPERIMENTAL

According to the following equation, the starting material for the synthesis of χ-$DyBO_3$ and χ-$ErBO_3$ in this work was a 1:1 molar mixture of B_2O_3 (from H_3BO_3 (99.8%, Merck, Darmstadt) fired at 600°C) with the rare-earth oxides Dy_2O_3 and Er_2O_3 (Dy_2O_3, Er_2O_3: 99.9%, Sigma-Aldrich, Taufkirchen), respectively.

$$Ln_2O_3 + B_2O_3 \xrightarrow[1600\ \mathrm{K}]{8.0\ \mathrm{GPa}} 2\chi\text{-}LnBO_3 \quad (Ln = \mathrm{Dy, Er}). \quad [1]$$

The compounds were mixed thoroughly under air and loaded into a 2.70 mm outside diameter, 0.35 mm wall thickness, and 4.0 mm length hexagonal boron nitride cylinder that was sealed by a BN plate. The sample cylinder was placed in the center of a cylindrical resistance heater (graphite) that had a variable (stepped) wall thickness in order to minimize the thermal gradient along the sample (12–15). MgO rods filled the space at the top and the bottom of the sample. A cylindrical zirconia sleeve surrounding the furnace provided thermal insulation. As pressure medium,

TABLE 1
Crystal Data and Structure Refinement for χ-$Ln$$BO_3$ (Ln = Dy, Er)

Empirical formula	χ-$DyBO_3$	χ-$ErBO_3$
Molar mass (g/mol)	221.31	226.07
Crystal system	triclinic	
Space group	$P\bar{1}$ (no. 2)	
Diffractometer	Enraf–Nonius Kappa CCD	
Radiation	Mo$K\alpha$ (λ = 71.073 pm)	
Unit cell dimensions	a = 724.0(1) pm	a = 718.1(1) pm
	b = 901.1(1) pm	b = 897.1(1) pm
	c = 987.2(1) pm	c = 980.2(1) pm
	α = 81.40(2)°	α = 81.32(2)°
	β = 85.67(2)°	α = 85.54(2)°
	γ = 77.02(2)°	γ = 77.11(2)°
Volume (nm^3)	0.620	0.608
Formula units per cell	Z = 12	
Calculated density (g/cm^3)	7.113	7.411
Crystal size (mm^3)	0.04 × 0.04 × 0.08	0.02 × 0.02 × 0.04
Detector distance (mm)	30.0	30.0
Exposure time/deg (s)	20	280
Absorption coefficient (mm^{-1})	35.8	41.1
F(000)	1140	1164
θ range	3.5–35°	
Range in $h\,k\,l$	±11, ±14, ±15	
Scan type	ω	φ/ω
Total no. of reflections	19,393	20,245
Independent reflections	5341 (R_{int} = 0.0817)	5358 (R_{int} = 0.0708)
Reflections with $I > 2\sigma(I)$	4335 (R_{sigma} = 0.0587)	4272 (R_{sigma} = 0.0520)
Data/parameters	5341/272	5358/272
Absorption correction	Numerical (HABITUS (27))	
Transm. ratio (max/min)	3.50	1.76
Goodness-of-fit on F^2	1.017	1.033
Final R indices [$I > 2\sigma(I)$]	$R1$ = 0.0349	$R1$ = 0.0323
	w$R2$ = 0.0877	w$R2$ = 0.0761
R indices (all data)	$R1$ = 0.0448	$R1$ = 0.0452
	w$R2$ = 0.0922	w$R2$ = 0.0807
R (subcell reflections)[a]	2671 > 0$\sigma(F)$, $R1$ = 0.0340	2680 > 0$\sigma(F)$, $R1$ = 0.0300
R (supercell reflections)[a]	2670 > 0$\sigma(F)$, $R1$ = 0.0902	2678 > 0$\sigma(F)$, $R1$ = 0.1052
Extinction coefficient	0.00260(12)	0.00070(7)
Largest diff. peak and hole ($e/Å^3$)	5.03 and −4.68	3.69 and −3.11

[a]These values were calculated with the program RWERT (28) using the formula $R = \sum|F_o - F_c|/\sum|F_o|$.

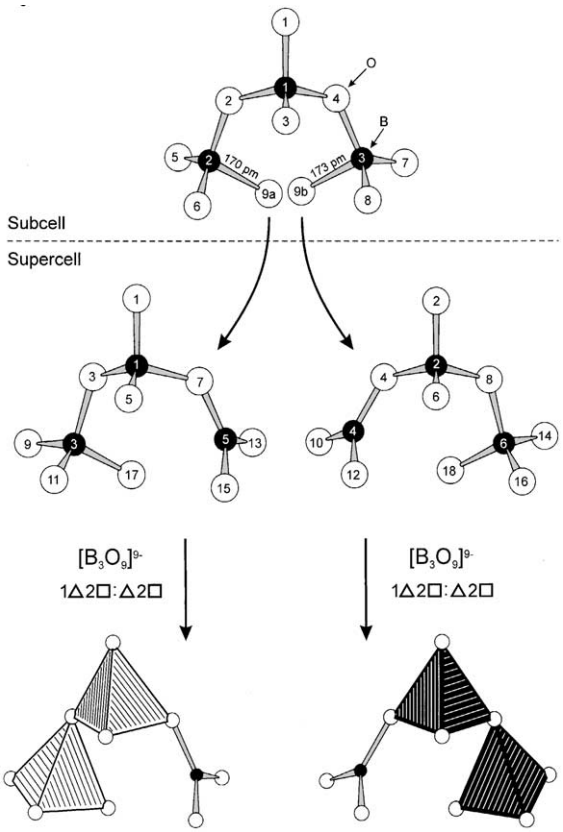

FIG. 1. The subcell- solution (top) of the crystal structures of χ-$Ln$$BO_3$ (Ln = Dy, Er) leads to a split oxygen atom (9a and 9b) with unusually long B–O bond lengths of 170 and 173 pm in the $[B_3O_9]^{9-}$-unit. Solution and refinement of the superstructure (center) exhibited two crystallographically independent $[B_3O_9]^{9-}$-anions each consisting of one trigonal BO_3- and two tetrahedral BO_4-groups. The left $[B_3O_9]^{9-}$-unit including the boron atoms B1, B2, and B3 is drawn as white polyhedra, while the right unit (B4, B5, and B6) is plotted as black polyhedra (bottom).

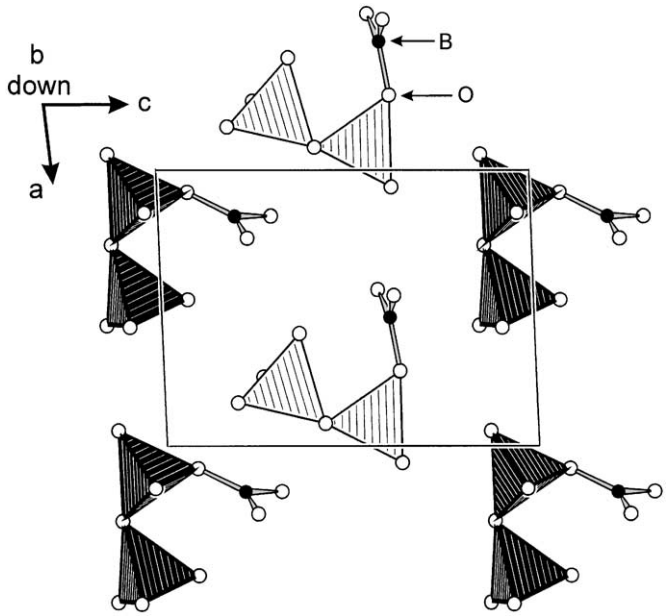

FIG. 2. Layer of isolated $[B_3O_9]^{9-}$-anions in χ-$Ln$$BO_3$ (Ln = Dy, Er); view along [010].

Cr_2O_3-doped MgO octahedra (Ceramic Substrates and Components LTD., Isle of Wight) with an edge length of 14 mm were used. A hole was drilled in the octahedron, the cylindrical assembly positioned inside and contacted with a molybdenum ring at the top and a molybdenum plate at the bottom. The experimental temperature was monitored using a $Pt/Pt_{87}Rh_{13}$ thermocouple that was inserted axially into the octahedral assembly with the hot junction in contact with the boron nitride cylinder. Eight tungsten carbide cubes separated by pyrophyllite gaskets (Plansee, Reutte, TSM10, edge length: 32 mm) with a truncation of 8 mm were used to compress the octahedron via a modified Walker-style split-cylinder multianvil apparatus (12). For further details concerning the Walker-type module and multianvil experiments see (12–15).

For the syntheses of χ-$Ln$$BO_3$ (Ln = Dy, Er) the assemblies were compressed to 8 GPa in 3 h and heated up to 1600 K in the following 10 min. After holding this temperature for 10 min, the sample was quenched by turning off the power with a quench rate of $>500^{\circ}C\,s^{-1}$. After decompression, the recovered experimental octahedron was broken apart and the sample carefully separated from the surrounding BN. χ-$DyBO_3$ was obtained as a colorless and χ-$ErBO_3$ as a light pink, crystalline phase. Quantitative analysis of χ-$DyBO_3$ concerning the elements dysprosium and boron with inductively coupled plasma (ICP) on a VARIAN-VISTA-Spectrometer led to 74.0 w% Dy (73.4%) and 5.4% B (4.9%) (theoretical values in parentheses).

3. CRYSTAL STRUCTURE ANALYSES

The powder patterns of χ-$Ln$$BO_3$ (Ln = Dy, Er) could be indexed on the basis of a primitive subcell with $a' = 616.4(2)$ pm, $b' = 716.1(2)$ pm, $c' = 723.4(3)$ pm, $\alpha' =$

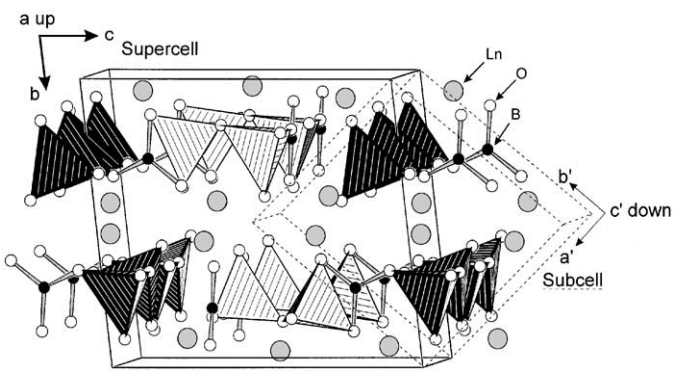

FIG. 3. Crystal structure of χ-$Ln$$BO_3$ (Ln = Dy, Er), view along [100]. Among one another the layers of isolated $[B_3O_9]^{9-}$-anions are related by a center of inversion. The subcell is drawn with dashed lines.

TABLE 2
Atomic Coordinates and Anisotropic Displacement Parameters (Å²) for χ-$DyBO_3$ (Space Group $P\bar{1}$). U_{eq} Is Defined as One Third of the Trace of the Orthogonalized U_{ij} Tensor

Atom	Wyckoff position	x	y	z	U_{11}	U_{22}	U_{33}	U_{23}	U_{13}	U_{12}	U_{eq}
Dy1	2*i*	0.5748(1)	0.0545(1)	0.1565(1)	0.0059(2)	0.0048(2)	0.0058(2)	−0.0002(1)	0.0003(1)	−0.0012(1)	0.00560(6)
Dy2	2*i*	0.4324(1)	0.4424(1)	0.3412(1)	0.0060(2)	0.0050(2)	0.0059(2)	0.0004(1)	0.0002(1)	−0.0013(1)	0.00577(6)
Dy3	2*i*	0.8999(1)	0.5651(1)	0.3295(1)	0.0057(2)	0.0048(2)	0.0054(2)	0.0001(1)	−0.0002(1)	−0.0012(1)	0.00536(6)
Dy4	2*i*	0.0998(1)	0.9309(1)	0.1632(1)	0.0057(2)	0.0050(2)	0.0057(2)	0.0001(1)	−0.0003(1)	−0.0012(1)	0.00555(6)
Dy5	2*i*	0.2494(1)	0.0482(1)	0.4774(1)	0.0064(2)	0.0069(2)	0.0064(2)	−0.0021(1)	−0.0003(1)	−0.0001(1)	0.00662(6)
Dy6	2*i*	0.7396(1)	0.4380(1)	0.0290(1)	0.0063(2)	0.0076(2)	0.0066(2)	−0.0023(1)	−0.0002(1)	−0.0004(1)	0.00685(7)
O1	2*i*	0.0611(5)	0.1845(4)	0.6298(3)	0.004(2)	0.006(2)	0.007(2)	−0.001(2)	0.000(2)	0.001(2)	0.0060(6)
O2	2*i*	0.9456(5)	0.3212(4)	0.8716(3)	0.005(2)	0.007(2)	0.008(2)	−0.002(2)	−0.001(2)	−0.001(2)	0.0067(6)
O3	2*i*	0.9186(5)	0.1623(4)	0.4266(3)	0.007(2)	0.007(2)	0.006(2)	0.001(2)	−0.001(2)	−0.001(2)	0.0069(6)
O4	2*i*	0.0821(5)	0.3342(4)	0.0803(3)	0.010(2)	0.006(2)	0.005(2)	0.000(2)	−0.001(2)	−0.001(2)	0.0071(6)
O5	2*i*	0.8492(5)	0.4115(4)	0.5357(4)	0.010(2)	0.003(2)	0.007(2)	0.001(2)	0.001(2)	−0.001(2)	0.0066(6)
O6	2*i*	0.1534(5)	0.0921(4)	0.9639(4)	0.009(2)	0.004(2)	0.009(2)	0.001(2)	0.000(2)	−0.003(2)	0.0073(6)
O7	2*i*	0.2703(5)	0.8164(4)	0.3658(3)	0.009(2)	0.009(2)	0.006(2)	0.000(2)	−0.001(2)	−0.005(2)	0.0073(6)
O8	2*i*	0.2729(5)	0.3227(4)	0.8729(3)	0.008(2)	0.006(2)	0.008(2)	0.000(2)	0.001(2)	−0.002(2)	0.0072(6)
O9	2*i*	0.8444(5)	0.1300(4)	0.1950(4)	0.009(2)	0.007(2)	0.010(2)	−0.006(2)	0.002(2)	0.000(2)	0.0088(6)
O10	2*i*	0.1665(5)	0.3639(4)	0.3028(4)	0.009(2)	0.008(2)	0.009(2)	−0.004(2)	0.000(2)	−0.002(2)	0.0087(6)
O11	2*i*	0.7525(5)	0.3835(4)	0.2658(4)	0.005(2)	0.005(2)	0.008(2)	−0.001(2)	−0.001(2)	−0.002(2)	0.0059(6)
O12	2*i*	0.2464(5)	0.1158(4)	0.2365(4)	0.007(2)	0.003(2)	0.009(2)	−0.001(2)	−0.001(2)	0.003(2)	0.0069(6)
O13	2*i*	0.4546(5)	0.0956(4)	0.6254(4)	0.006(2)	0.006(2)	0.010(2)	−0.001(2)	0.001(2)	−0.001(2)	0.0071(6)
O14	2*i*	0.4338(5)	0.5967(4)	0.1477(4)	0.012(2)	0.007(2)	0.009(2)	0.002(2)	−0.003(2)	−0.004(2)	0.0092(7)
O15	2*i*	0.5654(5)	0.6313(4)	0.4168(4)	0.006(2)	0.007(2)	0.008(2)	−0.001(2)	0.000(2)	0.000(2)	0.0074(6)
O16	2*i*	0.4287(5)	0.8733(4)	0.0862(4)	0.007(2)	0.002(2)	0.008(2)	0.001(2)	−0.002(2)	0.003(2)	0.0064(6)
O17	2*i*	0.5936(5)	0.1828(4)	0.3665(3)	0.010(2)	0.009(2)	0.009(2)	0.000(2)	0.001(2)	−0.002(2)	0.0096(6)
O18	2*i*	0.4702(5)	0.3129(4)	0.0712(4)	0.013(2)	0.010(2)	0.009(2)	0.000(2)	−0.003(2)	−0.002(2)	0.0107(7)
B1	2*i*	0.8915(8)	0.2468(6)	0.5518(6)	0.007(2)	0.006(2)	0.009(2)	0.002(2)	0.001(2)	−0.004(2)	0.0072(9)
B2	2*i*	0.1165(8)	0.2569(6)	0.9488(5)	0.005(2)	0.007(2)	0.006(2)	−0.001(2)	0.001(2)	−0.001(2)	0.0060(9)
B3	2*i*	0.7803(8)	0.2171(6)	0.3088(5)	0.007(2)	0.005(2)	0.005(2)	−0.003(2)	0.000(2)	0.001(2)	0.0060(9)
B4	2*i*	0.1669(8)	0.2709(6)	0.2052(6)	0.010(2)	0.005(2)	0.008(2)	−0.004(2)	0.001(2)	0.000(2)	0.0078(9)
B5	2*i*	0.5348(8)	0.2210(7)	0.6126(5)	0.008(2)	0.010(2)	0.004(2)	−0.001(2)	−0.001(2)	−0.001(2)	0.0073(9)
B6	2*i*	0.5240(8)	0.7157(6)	0.0763(5)	0.008(2)	0.005(2)	0.008(2)	0.002(2)	−0.001(2)	−0.001(2)	0.0071(9)

101.12(3)°, $\beta' = 95.94(3)°$, $\gamma' = 95.26(3)°$, $V = 0.310\,nm^3$, $Z = 6$ for χ-$DyBO_3$ and $a' = 612.6(3)\,pm$, $b' = 712.9(5)\,pm$, $c' = 717.2(7)\,pm$, $\alpha' = 101.2(2)°$, $\beta' = 95.7(2)°$, $\gamma' = 94.9(2)°$, $V = 0.304\,nm^3$, $Z = 6$ for χ-$ErBO_3$. Small single crystals of both compounds isolated by mechanical fragmentation and examined by Buerger precession photographs revealed indeed weak superstructure reflections, which were not observable in the powder patterns. The lattice parameters are given in Table 1. The cell of the superstructure can be transformed to the subcell by the transformation matrix $(0\ -\frac{1}{2}\ \frac{1}{2},\ 0\ -\frac{1}{2}\ -\frac{1}{2},\ 100)$.

Single-crystal data were collected on an Enraf–Nonius Kappa CCD equipped with a rotating anode (Mo$K\alpha$ radiation). A numerical absorption correction (HABITUS (27)) was applied to the data. All relevant information concerning the data collection are listed in Table 1.

A systematic analysis of the superstructure data sets showed, that no systematic extinctions were observed, which is compatible with the space groups $P1$ and $P\bar{1}$. The centrosymmetric group was found to be correct during the structure refinement. The starting positional parameters were deduced from an automatic interpretation of direct methods with SHELXS-97 (16) and the structure was successfully refined with anisotropic atomic displacement parameters for all atoms using SHELXL-97 (full-matrix least squares on F^2) (17). The solution in the subcell led to unreasonable B–O bond lengths (Fig. 1, top), which was clarified by the solution and refinement of the superstructure. Final difference Fourier syntheses revealed no significant residual peaks (see Table 1). The positional parameters and interatomic distances of the refinements are listed in Tables 2–7. Listings of the observed/calculated structure factors and other details are available from the Fachinformationszentrum Karlsruhe, D-76344 Eggenstein-Leopoldshafen (Germany), e-mail: crysdata@fiz-karlsruhe.de, by quoting the registry number CSD-412169 for χ-$DyBO_3$ and CSD-412168 for χ-$ErBO_3$.

4. RESULTS AND DISCUSSION

The subcell solution of the solid-state structures of the rare-earth orthoborates χ-$LnBO_3$ (Ln = Dy, Er) implied

TABLE 3
Interatomic Distances (pm) Calculated with the Single-Crystal Lattice Parameters in χ-$DyBO_3$

Dy1–O9	228.1(3)	Dy2–O14	218.9(3)	Dy3–O11	232.5(3)
Dy1–O18	232.9(4)	Dy2–O10	227.0(3)	Dy3–O5a	233.7(3)
Dy1–O16a	234.4(3)	Dy2–O11	234.8(4)	Dy3–O10	236.1(4)
Dy1–O13	238.8(3)	Dy2–O17	235.3(4)	Dy3–O5b	239.5(3)
Dy1–O16b	238.8(3)	Dy2–O15a	236.8(3)	Dy3–O8	240.5(3)
Dy1–O12	241.6(4)	Dy2–O15b	238.2(4)	Dy3–O2	241.2(3)
Dy1–O6	244.5(4)	Dy2–O5	250.3(4)	Dy3–O1	243.1(3)
Dy1–O17	254.6(3)			Dy3–O15	248.1(4)
Dy4–O9	230.8(4)	Dy5–O1	226.3(4)	Dy6–O2	227.6(4)
Dy4–O6a	232.6(3)	Dy5–O13a	230.7(3)	Dy6–O11	232.0(3)
Dy4–O6b	236.1(3)	Dy5–O12	236.5(4)	Dy6–O14a	232.0(3)
Dy4–O12	238.7(3)	Dy5–O3a	244.3(3)	Dy6–O18a	244.4(3)
Dy4–O7	240.3(3)	Dy5–O13b	247.4(4)	Dy6–O8	247.4(3)
Dy4–O16	241.0(4)	Dy5–O7	247.4(4)	Dy6–O4a	250.7(3)
Dy4–O2	244.4(3)	Dy5–O17	249.8(3)	Dy6–O18b	252.1(4)
Dy4–O1	248.3(3)	Dy5–O3b	251.0(3)	Dy6–O14b	264.7(4)
				Dy6–O4b	271.4(3)
B1–O5	143.3(7)	B3–O9	145.4(6)	B5–O13	136.8(6)
B1–O1	145.6(6)	B3–O11	146.9(6)	B5–O15	136.6(7)
B1–O3	152.5(7)	B3–O17	150.5(6)	B5–O7	140.0(6)
B1–O7	154.1(6)	B3–O3	154.2(6)		**∅ = 137.8**
	∅ = 148.9		**∅ = 149.3**		
B2–O6	143.6(7)	B4–O10	136.8(6)	B6–O16	144.7(7)
B2–O2	146.1(6)	B4–O12	138.5(7)	B6–O14	144.7(6)
B2–O8	149.6(6)	B4–O4	140.4(6)	B6–O18	151.2(6)
B2–O4	154.2(6)		**∅ = 138.6**	B6–O8	153.7(6)
	∅ = 148.4				**∅ = 148.6**

Note. Standard deviations in parentheses. The letters a and b indicate symmetry equivalent oxygen atoms, which coordinate to the corresponding Dy^{3+} in different interatomic distances.

a cyclic $[B_3O_9]^{9-}$-unit built up by three corner-sharing BO_4-tetrahedra ($3\square{:}\langle 3\square\rangle$), which is quite common in borate crystal chemistry (18). Further refinement of the subcell showed, that one of the bridging oxygen atoms in the ring (O9) had to be split to O9a and O9b (Fig. 1, top) leading to an open circle with two unusually long B–O bond lengths of 170 pm (O9a–B2) and 173 pm (O9b–B3). The solution and refinement of the superstructure exhibited that the

TABLE 4
Interatomic Angles (deg) Calculated with the Single-Crystal Lattice Parameters in χ-$DyBO_3$

O5–B1–O1	110.5(4)	O9–B3–O11	112.0(4)	O15–B5–O13	123.4(4)
O5–B1–O3	120.4(4)	O9–B3–O17	108.6(4)	O15–B5–O7	123.1(4)
O1–B1–O3	105.8(4)	O11–B3–O17	108.2(4)	O13–B5–O7	113.5(4)
O5–B1–O7	110.6(4)	O9–B3–O3	110.4(4)		**∅ = 120.0**
O1–B1–O7	106.3(4)	O11–B3–O3	111.6(4)		
O3–B1–O7	102.1(3)	O17–B3–O3	105.7(4)		
	∅ = 109.3		**∅ = 109.4**		
O6–B2–O2	109.6(4)	O10–B4–O12	118.0(4)	O16–B6–O14	117.1(4)
O6–B2–O8	113.5(4)	O10–B4–O4	119.3(4)	O16–B6–O18	109.2(4)
O2–B2–O8	106.8(4)	O12–B4–O4	122.7(4)	O14–B6–O18	102.4(4)
O6–B2–O4	117.8(4)		**∅ = 120.0**	O16–B6–O8	112.5(4)
O2–B2–O4	104.9(4)			O14–B6–O8	105.7(4)
O8–B2–O4	103.4(4)			O18–B6–O8	109.4(4)
	∅ = 109.3				**∅ = 109.4**

Note. Standard deviations in parentheses.

TABLE 5
Atomic Coordinates and Anisotropic Displacement Parameters (Å^2) for χ-$ErBO_3$ (Space Group $P\bar{1}$. U_{eq} Is Defined as One-Third of the Trace of the Orthogonalized U_{ij} Tensor

Atom	Wyckoff position	x	y	z	U_{11}	U_{22}	U_{33}	U_{23}	U_{13}	U_{12}	U_{eq}
Er1	2*i*	0.5740(1)	0.0552(1)	0.1557(1)	0.0060(2)	0.0063(2)	0.0057(2)	− 0.0007(1)	0.0003(1)	− 0.0023(1)	0.00591(6)
Er2	2*i*	0.4333(1)	0.4421(1)	0.3426(1)	0.0061(2)	0.0062(2)	0.0062(2)	− 0.0004(1)	0.0001(1)	− 0.0022(1)	0.00608(6)
Er3	2*i*	0.9008(1)	0.5647(1)	0.3293(1)	0.0059(2)	0.0060(2)	0.0056(2)	− 0.0005(1)	− 0.0004(1)	− 0.0021(1)	0.00573(6)
Er4	2*i*	0.0989(1)	0.9316(1)	0.1631(1)	0.0058(2)	0.0063(2)	0.0056(2)	− 0.0006(1)	− 0.0004(1)	− 0.0020(1)	0.00580(6)
Er5	2*i*	0.2500(1)	0.0465(1)	0.4779(1)	0.0066(2)	0.0080(2)	0.0064(2)	− 0.0024(1)	− 0.0003(1)	− 0.0013(1)	0.00686(6)
Er6	2*i*	0.7383(1)	0.4392(1)	0.0291(1)	0.0061(2)	0.0087(2)	0.0066(2)	− 0.0027(1)	− 0.0001(1)	− 0.0017(1)	0.00698(6)
O1	2*i*	0.0633(5)	0.1843(4)	0.6302(3)	0.006(2)	0.010(2)	0.005(2)	− 0.002(2)	0.000(2)	− 0.001(2)	0.0068(6)
O2	2*i*	0.9433(6)	0.3193(4)	0.8717(4)	0.008(2)	0.010(2)	0.006(2)	0.000(2)	− 0.002(2)	− 0.003(2)	0.0082(6)
O3	2*i*	0.9199(5)	0.1611(4)	0.4274(4)	0.008(2)	0.006(2)	0.006(2)	− 0.001(2)	0.002(2)	− 0.002(2)	0.0066(6)
O4	2*i*	0.0807(6)	0.3362(4)	0.0806(4)	0.010(2)	0.007(2)	0.006(2)	− 0.001(2)	0.000(2)	− 0.002(2)	0.0075(6)
O5	2*i*	0.8495(6)	0.4127(4)	0.5350(4)	0.007(2)	0.006(2)	0.007(2)	0.000(2)	0.001(2)	0.000(2)	0.0072(6)
O6	2*i*	0.1537(5)	0.0912(4)	0.9640(4)	0.007(2)	0.006(2)	0.007(2)	− 0.001(2)	0.001(2)	− 0.001(2)	0.0066(6)
O7	2*i*	0.2694(6)	0.8173(4)	0.3636(4)	0.009(2)	0.009(2)	0.009(2)	− 0.002(2)	0.000(2)	− 0.004(2)	0.0084(7)
O8	2*i*	0.2721(5)	0.3233(4)	0.8721(4)	0.006(2)	0.006(2)	0.009(2)	− 0.001(2)	0.002(2)	− 0.004(2)	0.0069(6)
O9	2*i*	0.8430(6)	0.1291(4)	0.1948(4)	0.008(2)	0.010(2)	0.009(2)	− 0.004(2)	0.000(2)	− 0.002(2)	0.0086(7)
O10	2*i*	0.1664(6)	0.3657(4)	0.3035(4)	0.008(2)	0.011(2)	0.009(2)	− 0.006(2)	0.000(2)	− 0.002(2)	0.0087(7)
O11	2*i*	0.7529(6)	0.3841(4)	0.2651(4)	0.007(2)	0.005(2)	0.007(2)	0.000(2)	0.001(2)	− 0.002(2)	0.0065(6)
O12	2*i*	0.2454(6)	0.1159(4)	0.2377(4)	0.007(2)	0.006(2)	0.009(2)	− 0.001(2)	− 0.001(2)	− 0.002(2)	0.0069(6)
O13	2*i*	0.4531(5)	0.0952(4)	0.6264(4)	0.006(2)	0.007(2)	0.008(2)	− 0.001(2)	0.001(2)	− 0.004(2)	0.0069(6)
O14	2*i*	0.4349(6)	0.5945(4)	0.1485(4)	0.009(2)	0.008(2)	0.009(2)	0.000(2)	0.000(2)	− 0.005(2)	0.0083(7)
O15	2*i*	0.5664(5)	0.6310(4)	0.4169(4)	0.006(2)	0.005(2)	0.007(2)	0.000(2)	− 0.001(2)	0.000(2)	0.0065(6)
O16	2*i*	0.4284(6)	0.8732(4)	0.0871(4)	0.007(2)	0.008(2)	0.007(2)	− 0.003(2)	0.001(2)	− 0.002(2)	0.0073(6)
O17	2*i*	0.5924(5)	0.1836(4)	0.3673(4)	0.006(2)	0.010(2)	0.011(2)	0.000(2)	0.001(2)	− 0.005(2)	0.0085(7)
O18	2*i*	0.4716(6)	0.3108(4)	0.0724(4)	0.009(2)	0.008(2)	0.008(2)	0.000(2)	0.000(2)	− 0.002(2)	0.0082(7)
B1	2*i*	0.8916(9)	0.2477(7)	0.5520(6)	0.007(2)	0.008(2)	0.009(2)	− 0.004(2)	0.000(2)	− 0.002(2)	0.0076(9)
B2	2*i*	0.1172(8)	0.2571(6)	0.9483(6)	0.006(2)	0.006(2)	0.007(2)	0.001(2)	0.000(2)	− 0.001(2)	0.0068(9)
B3	2*i*	0.7793(9)	0.2186(6)	0.3093(6)	0.008(2)	0.006(2)	0.007(2)	− 0.003(2)	0.004(2)	− 0.003(2)	0.0070(9)
B4	2*i*	0.1687(9)	0.2715(7)	0.2058(6)	0.008(2)	0.007(2)	0.009(2)	0.001(2)	− 0.001(2)	− 0.001(2)	0.008(1)
B5	2*i*	0.5335(9)	0.2206(7)	0.6146(6)	0.007(2)	0.009(2)	0.009(2)	0.000(2)	− 0.002(2)	0.001(2)	0.009(1)
B6	2*i*	0.5226(8)	0.7149(6)	0.0770(6)	0.005(2)	0.007(2)	0.008(2)	0.000(2)	0.000(2)	− 0.002(2)	0.0064(9)

problematic oxygen atoms O9a and O9b shift towards the boron atoms B2 and B3 creating two crystallographically independent $[B_3O_9]^{9-}$-units (Fig. 1, center) which are non-cyclic. Both units are built up from one trigonal BO_3- and two tetrahedral BO_4-groups. The B–O bond lengths in the non-planar BO_3-groups of both compounds vary between 136 and 141 pm (Tables 3 and 6) with a mean value of 138 pm which is in good agreement with the average B–O distance of 137 pm (19) in planar and non-planar BO_3-units. The O–B–O angles are between 113 and 124° (Tables 4 and 7). In the tetrahedral BO_4-groups of χ-$DyBO_3$ and χ-$ErBO_3$, the B–O distances shift between 143 and 155 pm which is also consistent to the average B–O distance of 147 pm (19) in tetrahedral BO_4-units of oxoborates (Tables 3 and 6). The O–B–O angles in the BO_4-tetrahedra are between 102 and 121° (Tables 4 and 7), whereby the upper value is remarkablly high. For comparison, the O–B–O angles in tetragonal γ-$LiBO_2$ prepared at 1.5 GPa and 950°C do not exceed 114° (20). The BO_4-tetrahedra in χ-$DyBO_3$ and χ-$ErBO_3$ obviously start to distort at a pressure of 8 GPa.

To our knowledge, all discrete $[B_3O_9]^{9-}$-anions described in the literature form rings consisting of three tetrahedral BO_4-groups (3□:⟨3□⟩). This is confirmed by a recent review of Becker, who gave a list of fundamental building blocks after screening over 460 anhydrous oxoborates (18). Here, we found for the first time the new non-cyclic $[B_3O_9]^{9-}$-anion, which can be written as 1Δ2□:Δ2□. In this style, introduced by Burns *et al.* (21, 22), the descriptor Δ stands for a BO_3-unit and □ for a BO_4-tetrahedron. Known discrete fundamental building blocks for anhydrous borates with three polyhedra are 3Δ:⟨3Δ⟩, 2Δ1□:⟨2Δ□⟩, 2Δ1□:Δ□Δ, and the above-mentioned 3□:⟨3□⟩ (18). In hydrous borates also the three-membered ring 1Δ2□:⟨Δ2□⟩ exists, which seems to be favored relative to the other possible combinations.

A better understanding of the structures of χ-$Ln$$BO_3$ (Ln = Dy, Er) can be reached by drawing the first $[B_3O_9]^{9-}$-unit including the boron atoms B1, B2, and B3 as white polyhedra, while the other unit (B4, B5, and B6) is plotted as black polyhedra. In the solid-state

TABLE 6
Interatomic Distances (pm) Calculated with the Single-Crystal Lattice Parameters in χ-$ErBO_3$

Er1–O9	225.4(4)	Er2–O14	216.9(4)	Er3–O11	230.9(3)
Er1–O18	228.9(4)	Er2–O10	225.1(4)	Er3–O5a	231.0(4)
Er1–O16a	232.7(4)	Er2–O11	233.0(4)	Er3–O10	233.0(4)
Er1–O13	236.7(4)	Er2–O17	233.1(4)	Er3–O5b	237.5(4)
Er1–O16b	237.0(4)	Er2–O15a	234.9(4)	Er3–O8	238.2(4)
Er1–O12	240.3(4)	Er2–O15b	235.0(4)	Er3–O2	240.4(4)
Er1–O6	242.7(4)	Er2–O5	248.5(4)	Er3–O1	241.7(3)
Er1–O17	254.5(4)			Er3–O15	246.0(4)
Er4–O9	228.9(4)	Er5–O1	225.0(4)	Er6–O2	226.8(4)
Er4–O6a	230.3(4)	Er5–O13a	229.0(3)	Er6–O11	229.7(4)
Er4–O6b	234.0(4)	Er5–O12	234.3(4)	Er6–O14a	230.9(4)
Er4–O7	237.1(3)	Er5–O3a	242.2(4)	Er6–O18a	242.6(4)
Er4–O12	237.4(3)	Er5–O7	245.8(4)	Er6–O8	245.5(3)
Er4–O16	239.1(4)	Er5–O13b	246.0(4)	Er6–O4a	248.8(4)
Er4–O2	241.4(4)	Er5–O17	247.5(4)	Er6–O18b	251.8(4)
Er4–O1	246.6(4)	Er5–O3b	247.6(3)	Er6–O14b	260.8(4)
				Er6–O4b	268.4(4)
B1–O5	143.0(7)	B3–O9	146.3(6)	B5–O13	136.1(7)
B1–O1	146.1(7)	B3–O11	145.7(6)	B5–O15	136.6(7)
B1–O3	152.1(6)	B3–O17	149.6(7)	B5–O7	140.5(7)
B1–O7	153.8(7)	B3–O3	154.7(7)		**∅ = 137.7**
	∅ = 148.8		**∅ = 149.1**		
B2–O6	143.9(6)	B4–O10	136.6(7)	B6–O16	144.5(7)
B2–O2	146.4(7)	B4–O12	137.9(7)	B6–O14	143.6(7)
B2–O8	147.6(7)	B4–O4	140.9(7)	B6–O18	151.3(6)
B2–O4	154.7(6)		**∅ = 138.5**	B6–O8	154.2(7)
	∅ = 148.2				**∅ = 148.4**

Note. Standard deviations in parentheses. The letters a and b indicate symmetry equivalent oxygen atoms, which coordinate to the corresponding Er^{3+} in different interatomic distances.

χ-$Ln BO_3$ (Ln = Dy, Er) is built up from layers of isolated $[B_3O_9]^{9-}$-units (Fig. 2). Among one another, these layers are related by a center of inversion. The lanthanoide atoms (Ln = Dy, Er) are situated between the layers (Fig. 3). The metal ions are coordinated by seven, eight, and nine oxygen atoms (Fig. 4). The Ln–O-distances (Ln = Dy, Er) vary between 217 and 271 pm (Tables 3 and 6), whereby the bond-valence sums around the Ln^{3+} cations do not deviate significantly from their ideal values.

TABLE 7
Interatomic Angles (deg) Calculated with the Single-Crystal Lattice Parameters in χ-$ErBO_3$

O5–B1–O1	110.9(4)	O9–B3–O11	112.2(4)	O15–B5–O13	123.6(5)
O5–B1–O3	120.8(4)	O9–B3–O17	107.8(4)	O15–B5–O7	123.1(5)
O1–B1–O3	104.9(4)	O11–B3–O17	108.8(4)	O13–B5–O7	113.4(5)
O5–B1–O7	111.3(4)	O9–B3–O3	109.5(4)		**∅ = 120.0**
O1–B1–O7	105.5(4)	O11–B3–O3	112.5(4)		
O3–B1–O7	101.9(4)	O17–B3–O3	105.7(4)		
	∅ = 109.2		**∅ = 109.4**		
O6–B2–O2	108.7(4)	O10–B4–O12	118.6(5)	O16–B6–O14	118.3(5)
O6–B2–O8	113.9(4)	O10–B4–O4	118.3(5)	O16–B6–O18	108.5(4)
O2–B2–O8	107.4(4)	O12–B4–O4	122.9(5)	O14–B6–O18	103.1(4)
O6–B2–O4	118.1(4)		**∅ = 119.9**	O16–B6–O8	111.9(4)
O2–B2–O4	104.4(4)			O14–B6–O8	105.1(4)
O8–B2–O4	103.5(4)			O18–B6–O8	109.4(4)
	∅ = 109.3				**∅ = 109.4**

Note. Standard deviations in parentheses.

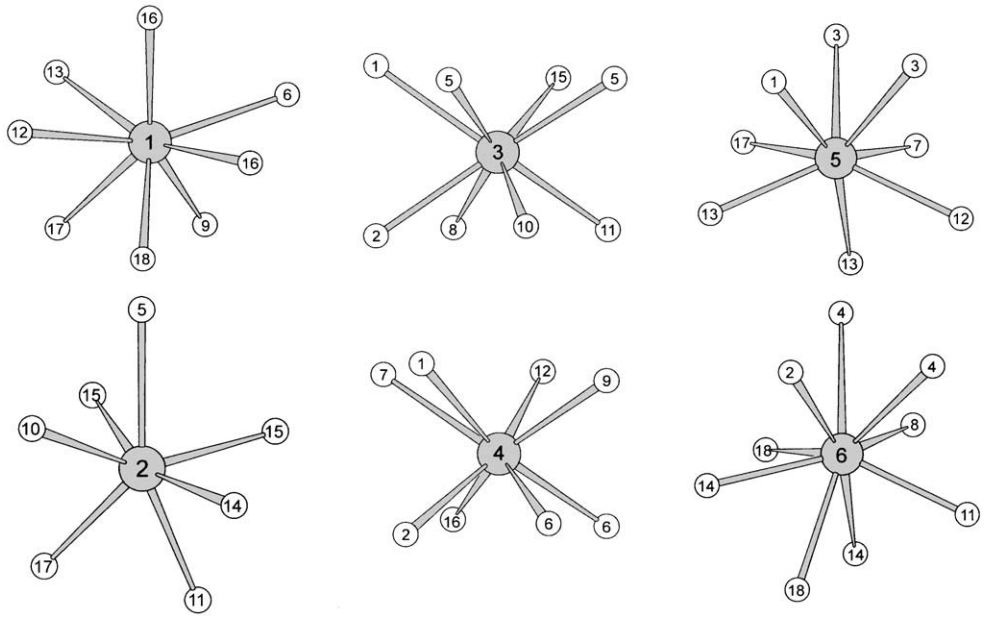

FIG. 4. Coordination polyhedra of Ln^{3+} (gray spheres) in the crystal structures of χ-$Ln$$BO_3$ (Ln = Dy, Er).

In comparison with the known rare-earth orthoborates $Ln$$BO_3$, which exhibit isolated planar/non-planar BO_3 or cyclic $[B_3O_9]^{9-}$-anions, we observe the coexistence of both BO_3 and BO_4 units in the polymorphs χ-$DyBO_3$ and χ-$ErBO_3$.

4.1. *In Situ Powder Diffraction*

To investigate the metastable character of the high-pressure phase χ-$DyBO_3$, temperature-dependent measurements were performed on a STOE powder diffractometer

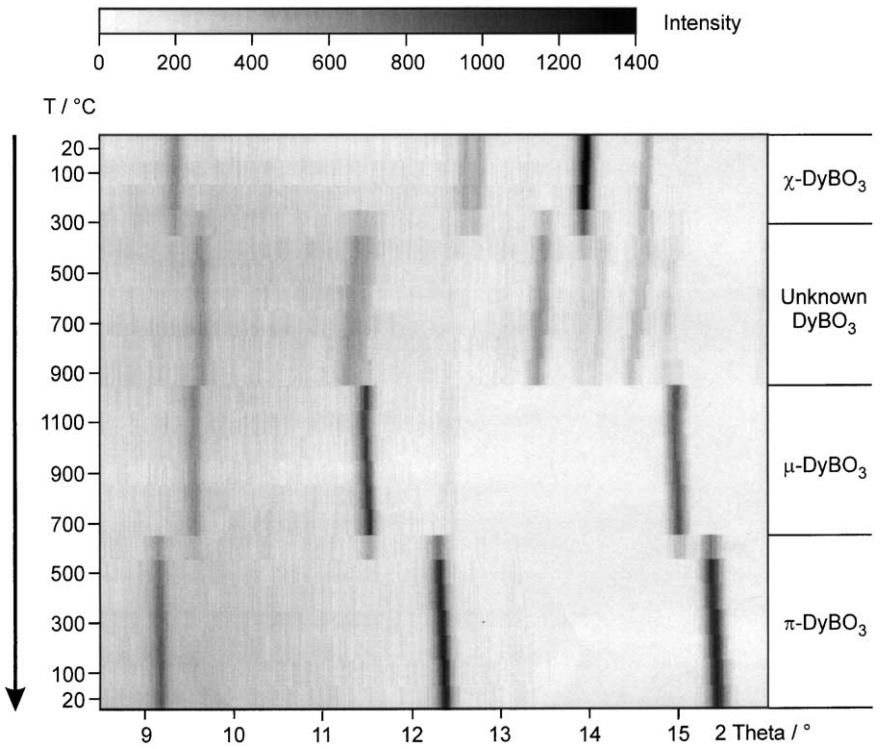

FIG. 5. Temperature-dependent X-ray thermodiffractometric powder patterns (λ = 71.073 pm) of the phase transitions of χ-$DyBO_3$.

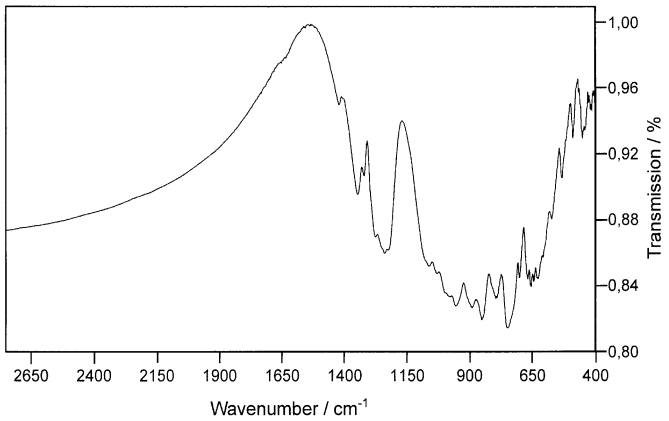

FIG. 6. Infrared spectrum of χ-$DyBO_3$.

Stadi P (Mo$K\alpha$; $\lambda = 71.073$ pm) with a computer-controlled STOE furnace. The heating element consisted of an electrically heated graphite tube holding the sample capillary vertically with respect to the scattering plane. Bores in the graphite tube permited unobstructed pathways for the primary beam as well as for the scattered radiation. The temperature measured by a thermocouple in the graphite tube was kept constant to within 0.2°C. The heating rate between different temperatures was set to 22°C/min. For temperature stabilization, a time of 3 min was given before starting each data acquisition. Successive heating of the metastable high-pressure phase χ-$DyBO_3$ (Fig. 5) leads in the range of 300°C to a phase transformation into an unknown phase, which transforms to the high-temperature phase μ-$DyBO_3$ (3) at 1000°C. Subsequent cooling shows the transformation of μ-$DyBO_3$ to the low-temperature phase π-$DyBO_3$ (3) below 600°C.

4.2. Infrared Absorption Spectroscopy

The infrared (IR) spectrum of χ-$DyBO_3$ (Fig. 6) was recorded on a Bruker IFS 66v/S spectrometer scanning a range from 400 to 4000 cm^{-1}. The sample was thoroughly mixed with dried KBr (5 mg sample, 500 mg KBr) in a glove box under dried argon atmosphere.

Figure 6 shows the section 400–2750 cm^{-1} of the IR spectrum. The absorption peaks between 790 and 1100 cm^{-1} are those typical for the tetrahedral borate group BO_4 as in YBO_3, $GdBO_3$, or $TaBO_4$ (6, 23, 24). The typical absorptions of the triangular BO_3-groups appear at about 1240 cm^{-1} and below 790 cm^{-1} as in $LaBO_3$ (25, 26). Due to the combination of one BO_3- and two BO_4-units in the $[B_3O_9]^{9-}$-unit and the presence of two crystallographically independent anions in the solid state, a detailed assignment of the vibrations is difficult. In the upper range (4000–2750 cm^{-1}) no absorption bands due to hydrogen (OH) were detectable.

5. CONCLUSION

In this paper, we have described the syntheses of two new orthoborates χ-$DyBO_3$ and χ-$ErBO_3$ via multianvil high-pressure syntheses. The superstructures were solved from single-crystal X-ray diffraction data. Both compounds are built up from layers of isolated $[B_3O_9]^{9-}$-units. Normally, discrete $[B_3O_9]^{9-}$-anions described in the literature form rings consisting of three tetrahedral BO_4-groups ($3\square:\langle 3\square\rangle$). In these compounds, we found for the first time that the $[B_3O_9]^{9-}$-anions are built up by one BO_3-triangle and two BO_4-tetrahedra and do not form a ring but a new discrete fundamental building block corresponding to $1\triangle 2\square:\triangle 2\square$.

ACKNOWLEDGMENTS

We thank Prof. Dr. W. Schnick, Department Chemie of the University of Munich (LMU), for his steady interest and continuous support of this work. Special thanks go to Dipl. Chem. S. Correll for the *in situ* powder diffraction measurements.

REFERENCES

1. P. Becker, *Adv. Mater.* **10,** 979 (1998).
2. "Gmelin Handbook of Inorganic and Organometallic Chemistry C11b" (H. Bergmann, Ed.), 8th ed., Springer-Verlag, Berlin, 1991.
3. E. M. Levin, R. S. Roth, and J. B. Martin, *Am. Mineral. J.* **46,** 1030, (1961).
4. R. S. Roth, J. L. Waring, and E. M. Levin, "Proceedings of the Third Conference Rare Earth Research, Clearwater, FLA, p. 153." (1963).
5. G. Chadeyron, M. El-Ghozzi, R. Mahiou, A. Arbus, and J. C. Cousseins, *J. Solid State Chem.* **128,** 261, (1997).
6. M. Ren, J. H. Lin, Y. Dong, L. Q. Yang, M. Z. Su, and L. P. You, *Chem. Mater.* **11,** 1576 (1999).
7. R. Böhlhoff, H. U. Bambauer, and W. Hoffmann, *Z. Kristallogr.* **133,** 386 (1971).
8. K. K. Palkina, V. G. Kuznetsov, L. A. Butman, and B. F. Dzhurinskii, *Acad. Sci. USSR* **2,** 286, (1976).
9. H. J. Meyer, *Naturwissenschaften* **56,** 458 (1969).
10. H. J. Meyer, *Naturwissenschaften* **59,** 215 (1972).
11. H. J. Meyer and A. Skokan, *Naturwissenschaften* **58,** 566 (1971).
12. H. Huppertz, *Z. Naturforsch.* **56b,** 697 (2001).
13. D. Walker, M. A. Carpenter, and C. M. Hitch, *Am. Mineral. J.* **75,** 1020 (1990).
14. D. Walker *Am. Mineral.* **76,** 1092 (1991).
15. D. C. Rubie, *Phase Trans.* **68,** 431 (1999).
16. G. M. Sheldrick, "SHELXS-97, Program for the Solution of Crystal Structures." University of Göttingen, Germany, 1997.
17. G. M. Sheldrick, "SHELXL-97, Program for Crystal Structure Refinement." University of Göttingen, Germany, 1997.
18. P. Becker, *Z. Kristallogr.* **216,** 523 (2001).
19. F. C. Hawthorne, P. C. Burns, and J. D. Grice, *in* "Boron: Mineralogy, Petrology, and Geochemistry" (E. S. Grew and L. M. Anovitz, Eds.), Chap. 2. Reviews in Mineralogy 33. Mineralogical Society of America, Washington, 1996.
20. M. Marezio and J. P. Remeika, *J. Chem. Phys.* **44,** 3348 (1966).
21. P. C. Burns, J. D. Grice, and F. C. Hawthorne, *Can. Mineral.* **33,** 1131 (1995).
22. P. C. Burns, J. D. Grice, and F. C. Hawthorne, *Can. Mineral.* **37,** 731 (1999).

23. J. P. Laperches and P. Tarte, *Spectrochim. Acta* **22,** 1201 (1966).
24. G. Blasse and G. P. M. van den Heuvel, *Phys. Stat Sol* **19,** 111 (1973).
25. W. C. Steele and J. C. Decius, *J. Chem. Phys.* **25,** 1184 (1956).
26. R. Böhlhoff, H. U. Bambauer, and W. Hoffmann, *Z. Kristallogr.* **133,** 386 (1971).
27. W. Herrendorf and H. Bärnighausen, "HABITUS, Program for Numerical Absorption Correction." University of Karlsruhe/Gießen, Germany, 1993/1997.
28. R.-D. Hoffmann, "RWERT, Program for the Calculation of *R* Values for Specific Classes of Reflections." University of Münster, Germany, 1996.